



Validating Kraken for VVER-1000 fuel cycle simulations using the X2 benchmark

Ville Valtavirta ^{*}, Antti Rintala

VTT Technical Research Centre of Finland Ltd, P.O. Box 1000, VTT, 02044, Finland



ARTICLE INFO

Keywords:

Kraken
Ants
Serpent
Fuel cycle
VVER-1000
X2 benchmark

ABSTRACT

This article contributes to the validation of the Kraken framework for VVER-1000 fuel cycle modelling. Four fuel cycles from the X2 VVER-1000 benchmark are simulated along with the start-up tests at the beginning of each cycle. Predicted boron letdown curves, power distributions and start-up test results for the four fuel cycles are compared to measured data from the benchmark as well as the results of similar reactor analysis tools. The comparisons to measured data show that Kraken performs well in the task. The accuracy of Kraken is comparable to other nodal diffusion based solvers.

1. Introduction

Kraken (Leppänen et al., 2022) is VTT's new reactor analysis framework. It replaces legacy solvers with modern ones such as the two step neutronics calculation chain based on the Serpent Monte Carlo code (Leppänen et al., 2015) and the Ants nodal neutronics program (Sahlberg and Rintala, 2018; Rintala and Sahlberg, 2019). Kraken is intended to cover VTT's current and future reactor analysis needs, which focus on the Finnish nuclear power plants, but also extend to upcoming new reactor concepts. In order to demonstrate the capability of Kraken to conduct relevant fuel cycle and transient analyses, international benchmarks are utilized in the verification and validation work.

The verification of the Serpent–Ants neutronics chain for hexagonal lattice applications started with several international numerical hexagonal geometry benchmarks with fixed group constants (Rintala and Sahlberg, 2019). Computational verification for Ants assembly and pin power predictions for several VVER-440 and VVER-1000 benchmarks against a Serpent reference solution were recently published (Valtavirta et al., 2022b). The experimental verification for the Serpent–Ants calculation chain have started with simulations of the initial start-up tests of the Khmelnitsky 2 (X2) nuclear power plant (Valtavirta et al., 2022a).

In this article we use the X2 benchmark (Lötsch et al., 2009, 2016; Bilodid et al., 2020) to validate the VVER-1000 fuel cycle simulation capabilities of Kraken by modelling the four fuel cycles included in the benchmark and comparing Kraken predictions for boron letdown, power distributions and start-up tests results to measured and reconstructed data from the benchmark as well as to predictions from other reactor analysis tools. This process not only tests the capabilities of

Kraken to model multi-cycle operation of a VVER-1000 reactor and the associated start-up tests but also provides quantitative estimates of the accuracy of Kraken compared to the measured data and other similar tools. Section 2 gives an overview of the relevant parts of the X2 benchmark and Section 3 describes the applied codes of the Kraken framework. Section 4 describes the calculation setup including the group constant generation process. Section 5 presents the main results and discusses the comparisons between the predicted and measured or reconstructed data as well as the comparisons with other computational solutions to the benchmark.

2. The X2 benchmark

The X2 benchmark was originally proposed by Lötsch et al. (2009) as a core burnup benchmark based on operating cycle data from the recently started Khmelnitsky nuclear power plant unit 2. Updated specifications were published by Lötsch et al. (2010) with the benchmark updated to contain two tasks: the preparation of the fuel assembly data (group constant generation) and 3D burnup calculations (operating cycle simulations). The benchmark was later extended to also cover the start-up tests conducted at the beginning of each operating cycle and to 3D reactor dynamics calculations based on several transient test scenarios from the unit (Lötsch et al., 2016). Recently, revised specifications and a Monte Carlo reference solution for the fresh core start-up tests were published by Bilodid et al. (2020).

The benchmark extends over the first four operating cycles of a VVER-1000 reactor, in which the core consists of 163 hexagonal fuel assemblies with a hot active length of 355 cm. Fuel loading is based on

^{*} Corresponding author.

E-mail address: ville.valtavirta@vtt.fi (V. Valtavirta).

a variety of fuel assembly types with a range of uranium enrichment, various radial profiling patterns and gadolinia utilized as burnable absorber. The reactor has a nominal thermal power of 3000 MW.

X2 has been a popular benchmark for the verification of neutronics codes for VVER applications. The calculated results from the benchmark published by Lötsch et al. (2016) include several two-step chains: DYN3D (NESSEL group constants), DYN3D (CASMO group constants), TRAPEZ (NESSEL group constants) and BIPR7 A (TVSM group constants). More recent publications include the verification of SIMULATE5-HEX (Babadi, 2018) and RAST-V (Jang et al., 2022) for VVER applications and the verification of high fidelity tools such as NTF (Papadionysiou et al., 2022) and NECP-X (Liu et al., 2022).

The geometry and material data used in this work were based on the most recent specifications (Bilodid et al., 2020), which allow the construction of both the lattice homogenization models and the full core models. The specifications by Lötsch et al. (2010) provide the historical data required for modelling the first four operating cycles of the reactor with the actual power and control rod insertion history. The historical data includes reactor inlet mass flow rates and temperatures. The coolant soluble boron concentration is also provided for all of the history points. Finally, the specifications describe the shuffling of depleted fuel assemblies to new positions and the loading of several fresh assemblies into the core between fuel cycles.

The conditions for the start-up tests and the measurement results are described in the benchmark specifications for subtask 2.3. The data covers the evaluation of

- boron concentration in a critical reactor state
- scram worth with and without a stuck control rod assembly
- the isothermal temperature reactivity coefficient
- integral and differential reactivity worth of the working control rod group (group 10)

Additionally, reconstructed power distributions are provided for axially integrated fuel assembly powers at beginning of cycle (BOC), middle of cycle (MOC) and end of cycle (EOC) for each cycle (subtask 2.2) as well as reconstructed axial power distributions for several fuel assemblies in the BOC, MOC and EOC points of the four fuel cycles (subtask 3.1).

3. Methodology

3.1. Kraken

The Kraken reactor analysis framework (Leppänen et al., 2022) is intended to serve VTT in future deterministic safety analyses of the Finnish nuclear power plants. Additionally Kraken has been utilized in the design of the VTT's district heating reactor concept (Leppänen et al., 2021) and intended to be used also in more general reactor analysis and research tasks. The Kraken framework is based on the modular coupling of modern solvers for the reactor core level physics (neutronics, thermal hydraulics and fuel behaviour) and system scale solvers for plant level simulations. Fig. 1 shows the planned couplings in the Kraken framework with all but the coupling to the ENIGMA fuel performance solver already implemented.

Each solver module in the Kraken framework only needs to communicate with the central multi-physics driver Cerberus, which transfers data between the different modules and handles the general solution flow to achieve coupled stationary, depletion or transient solutions. The modularity of the framework provides the capability for consistent cross verification of the reduced order solvers of Kraken against high fidelity ones even in coupled calculations (Valtavirta et al., 2020; Valtavirta and Tuominen, 2021).

3.2. Neutronics

The neutronics solution in this work is based on the two step Serpent–Ants calculation chain, where the Serpent Monte Carlo code (Leppänen et al., 2015) is used to generate homogenized few-group constants for the Ants nodal neutronics program (Sahlberg and Rintala, 2018; Rintala and Sahlberg, 2019).

Serpent is the continuous energy Monte Carlo particle transport and burnup code developed at VTT since 2004. Overall, Serpent serves a dual role in the Kraken framework providing both the group constants for Ants and high fidelity reference neutronics solutions as in the X2 fresh core analysis presented recently by Valtavirta et al. (2022a).

The Ants nodal neutronics program has been developed at VTT since 2017 to replace legacy nodal neutronics codes at VTT. Developed from the start as a multi-group code, Ants is based on a combination of the analytic function expansion nodal method (AFEN) and flux expansion nodal method (FENM) to solve the multi-group diffusion equation. Ants supports rectangular (Sahlberg and Rintala, 2018), hexagonal (Rintala and Sahlberg, 2019) and triangular (Hirvensalo et al., 2021) lattice geometries and is applicable to stationary, depletion and transient (Rintala and Lauranto, 2023) calculations.

The group constant generation for the X2 benchmark is described in Section 4.2.

3.3. Fuel behaviour

The nodal fuel temperatures required by Ants for the fuel temperature feedback on nodal group constants are evaluated by the SuperFINIX core level fuel behaviour solver (Valtavirta et al., 2019b). SuperFINIX receives the core level power distribution and thermal boundary condition from the multi-physics driver Cerberus and distributes the work of solving the fuel behaviour to individual instances of the FINIX fuel behaviour module (Ikonen et al., 2015). SuperFINIX collects the core level fuel temperature solution from the FINIX instances and passes it back to the multi-physics driver. SuperFINIX can be set up to model the reactor at pin level, explicitly considering each fuel rod in the core (Tuominen and Valtavirta, 2023) or at a more coarse level where average fuel rods are used for each assembly position or quarter assembly (Valtavirta et al., 2019a).

The FINIX fuel behaviour module has been developed at VTT for thermomechanical modelling of light water reactor fuel in multi-physics applications since 2012. FINIX calculates the thermomechanical solution for the cylindrical fuel rod separately for each axial segment. The radial heat equation is similarly solved separately for the axial segments. Different segments are only coupled together via the rod internal pressure. This approach of treating the axial segments separately in the thermal and mechanical solutions and coupling them via the internal pressure is often referred to as the 1.5 dimensional approach to fuel modelling.

3.4. Thermal hydraulics

Thermal hydraulics are modelled with Kharon, a closed-channel two-phase steady-state thermal hydraulics solver based on the porous medium approximation. Kharon was developed at VTT as a placeholder thermal hydraulics solver for initial testing in stationary and fuel cycle simulations. Kharon is well applicable for such simulations in geometries that have limited crossflow between adjacent coolant channels. For future applications a porous medium solver based on the OpenFOAM CFD toolbox is being introduced to the Kraken framework. This will provide the further capability to consider crossflows as well as transient scenarios.

In this work Kharon was used in single-phase mode to solve the coolant temperature and density as well as the cladding surface temperature based on the fission power distribution from Ants.

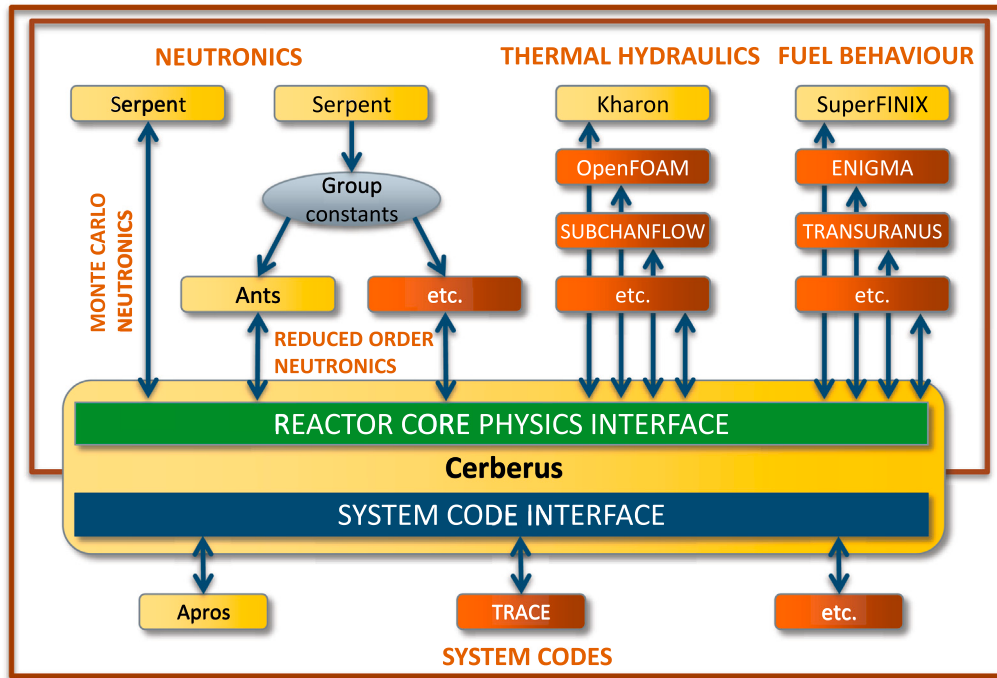


Fig. 1. A schematic representation of the plans for the completed Kraken framework. Finnish solver modules developed at VTT are shown in yellow and, while third party solvers to be coupled are shown in orange. All couplings to named solvers are already implemented except for the fuel performance code ENIGMA.

3.5. Operating cycle analyses

The operating cycle simulation is driven by the reactor simulator component in Kraken (Valtavirta and Tuominen, 2021), which handles the coupled iteration of each time point, the time integration process and evaluates peaking factors, axial offset and various other data such as reactivity coefficients if requested by the user.

4. Calculation setup

The following sections describe the spatial discretization applied in the different solvers, the group constant generation process used in the Serpent–Ants neutronics chain and the application of the fuel cycle boundary conditions from the tabulated data.

4.1. Nodal calculation models

The nodalization applied in the different solvers is illustrated in Fig. 2. The horizontal discretization of the problem was conducted at the assembly level: SuperFINIX modelled one average fuel rod per assembly, Kharon modelled one coolant channel per fuel assembly and Ants modelled each fuel assembly as a separate radial node accompanied with one assembly width of radial reflector nodes. The horizontal mapping between the different codes was thus one-to-one in the active core, and the coolant density and temperature for the Ants radial reflector nodes was taken from the Kharon inlet nodes below the active core.

The axial nodalization of Ants was largely based on material discontinuities in the reactor core. This is due to Ants currently using volume-weighting in the axial homogenization of group constants instead of the proper flux-volume weighting. Spacer grids and the specified structure of the bottom and top reflector were taken into account in the axial nodalization and the regions between spacer grids were divided into two nodes to yield non-gridded fuel nodes of 10.75 cm–12.75 cm height. All in all, the Ants model used 47 axial nodes, of which 41 were in the active core, 3 in the bottom reflector and 3 in the top reflector.

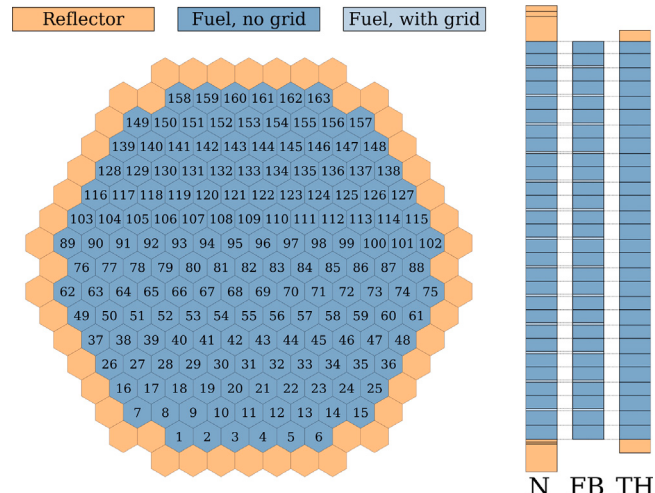


Fig. 2. Illustration of the horizontal nodalization of the problem with fuel assembly numbering and axial nodalization of the problem in the neutronics (N), fuel behaviour (FB) and thermal hydraulic (TH) solvers.

The fuel behaviour model matched the 41 axial nodes of Ants exactly in the active core and did not extend to the reflectors.

The thermal hydraulics model combined the short 2 cm spacer grid nodes with an adjacent non-grid node in order to avoid convergence issues from large changes in the node height. The thermal hydraulics model included one inlet node and one outlet node from which the thermal hydraulic data for the bottom and top reflector neutronics nodes were taken, respectively.

The field transfers between the neutronics and fuel behaviour solutions used a one-to-one mapping in the active core. The interpolation to and from the thermal hydraulics mesh was simple to set up as the thermal hydraulics mesh was obtained from the neutronics mesh by combining certain axial layers. The power of the combined cells was

a sum of the powers of the individual cells. The coolant density and temperature in the combined cell was applied as is in the individual cells making up the combined cell. The radial temperature distributions in the fuel pellet solved by the fuel behaviour module were condensed to neutronics temperatures by adjusting the NEA effective fuel temperature approach (Kozlowski and Downar, 2006) to use the pellet inner surface temperature in place of the pellet centreline temperature:

$$T_{\text{eff}} = 0.7 \times T_{\text{so}} + 0.3 \times T_{\text{si}}, \quad (1)$$

where T_{so} and T_{si} are the pellet outer and inner surface temperatures, respectively.

4.2. Group constants

4.2.1. Group constant model in Ants

While Ants supports multiple formats for group constant parametrization, this work uses the generic polynomial (GENPOLY) format, which is described in detail in a separate report (Valtavirta and Rintala, 2021). A short overview is given here to provide background for the following sections.

In the GENPOLY model, a group constant (Σ) is parametrized with respect to local burnup, local historical operating conditions and local momentary operating conditions.

The burnup dependence of data is modelled through the tabulation of the data at different burnups and the use of linear interpolation and extrapolation to obtain the data at a specific burnup $\Sigma(\text{bu})$.

Group constants are dependent on momentary local conditions such as fuel temperature, coolant density and coolant boron concentration. In the GENPOLY model, group constants are modelled with a user chosen polynomial dependence on such feedback variables. The nominal value of the group constant is evaluated by a lattice code at some nominal state of the feedback variables. The polynomial coefficients can be fitted by evaluating the value of the group constant also in a number of off-nominal momentary branch conditions. The polynomial fit coefficients are also tabulated with respect to burnup as is the nominal value of the group constant. However, the tabulated burnup points need not be the same for the nominal values and polynomial coefficients. The evaluation of the feedback effect on the group constant by evaluating the polynomial fit at some specific values of the feedback variables provides the feedback adjusted burnup dependent group constant value $\Sigma(\text{bu, fb})$.

The historical conditions of a fuel assembly affect its group constants via an effect on the nuclide content of the assembly. The GENPOLY model evaluates the history effect on the group constants using a plutonium history approach similar to that described by Bilodid et al. (2015). The atomic density of ^{239}Pu is tracked during the nodal calculation based on a simple microscopic depletion chain and is used to adjust the feedback adjusted burnup dependent group constant value to obtain the history and feedback adjusted burnup dependent group constant value $\Sigma(\text{bu, fb, his})$.

The effects of the short lived fission products on the homogenized macroscopic absorption cross sections are taken in account with simple chains. Both ^{135}I - ^{135}Xe chain and the ^{149}Pm - ^{149}Sm chain are modelled through depletion. ^{149}Pm production from ^{148}Pm and ^{148m}Pm is modelled assuming their nuclide densities to be in group constant generation calculation values (Ingremau et al., 2018).

The build-up of fission products and actinides other than those explicitly tracked by Ants is considered implicitly through the Serpent homogenization calculations being conducted using burnup dependent nuclide compositions.

Table 1
Conditions for group constant calculations.

	T fuel (K)	T cool (K)	ρ cool (g/cm ³)	Boron (ppm)
History calculations:				
Nominal	1005	578	0.7167	525
Off-nominal	1102.5	589	0.6893	1102.5
Branch calculations for HFP group constants				
Nominal	1005	578	0.7167	525
High T_f	1200	578	0.7167	525
Low T_f	600	578	0.7167	525
Zero boron	1005	578	0.7167	0
High boron	1005	578	0.7167	1500
High T_c , zero boron	1005	600	0.6618	0
Low T_c , zero boron	1005	550	0.7700	0
High T_c , high boron	1005	600	0.6618	1500
Low T_c , high boron	1005	550	0.7700	1500
Branch calculations for HZP group constants				
Nominal	554.15	554.15	0.7628	1000
Zero boron	554.15	554.15	0.7628	0
High boron	554.15	554.15	0.7628	1600
High T_c , zero boron	579.15	579.15	0.7142	0
Low T_c , zero boron	529.15	529.15	0.8030	0
High T_c , high boron	579.15	579.15	0.7142	1600
Low T_c , high boron	529.15	529.15	0.8030	1600

4.2.2. History and state point variations

The group constants for Ants were generated using the Serpent Monte Carlo code separately around the expected hot full power (HFP) and hot zero power (HZP) states of the reactor. The thermal hydraulic states covered by the Serpent calculations are shown in Table 1.

The polynomial fit used to describe the dependence of the group constants on the momentary values of state parameters around the HFP state was

$$\Sigma(\text{fb}) = \Sigma + c_1 \Delta \sqrt{T_f} + c_2 \left(\Delta \sqrt{T_f} \right)^2 + c_3 \Delta \rho_c + c_4 \left(\Delta \rho_c \right)^2 + c_5 \Delta \rho_b + c_6 \left(\Delta \rho_b \right)^2 + c_7 \rho_b \Delta \rho_c \quad (2)$$

where $\Sigma(\text{fb})$ is the feedback adjusted value for the group constant Σ is the nominal value of the group constant, c_i are polynomial coefficients and the Δ terms describe the deviation of the momentary state parameters from the nominal point for the square root of fuel temperature $\sqrt{T_f}$, coolant density ρ_c and boron mass density ρ_b .

The polynomial fit used around the HZP state was simpler due to only containing isothermal temperature variations:

$$\Sigma(\text{fb}) = \Sigma + c_1 \Delta \rho_c + c_2 \left(\Delta \rho_c \right)^2 + c_3 \Delta \rho_b + c_4 \left(\Delta \rho_b \right)^2 + c_5 \rho_b \Delta \rho_c. \quad (3)$$

4.2.3. Fuel assembly homogenization

Fuel assemblies were homogenized as two-dimensional infinite lattice models using 10^7 active neutron histories (50 inactive cycles) based on a previous study (Leppänen and Mattila, 2015). The infinite lattice model was based on a hexagonal unit cell coinciding with the assembly lattice and using periodic boundary conditions in the radial direction as illustrated in Fig. 3 for the assembly type 30AV5. Fuel assemblies were first depleted in nominal and off-nominal history conditions followed by branch calculations to each of the branch states using the depleted nuclide compositions separately from the nominal and off-nominal history calculations. The burnup calculations were conducted without spacer grid or control rod. The effect of spacer grid and control rod on the group constants was evaluated by running all of the branch calculations for all spacer grid and control rod configurations:

- No spacer present/spacer present.
- No control rod present/dysprosium titanate part of control rod present/boron carbide part of control rod present.

In the spacer branches, the spacer grids were modelled as an additional material layer on the cladding surface (according to Bilodid et al. (2020)) with a thickness that conserved the grid mass.

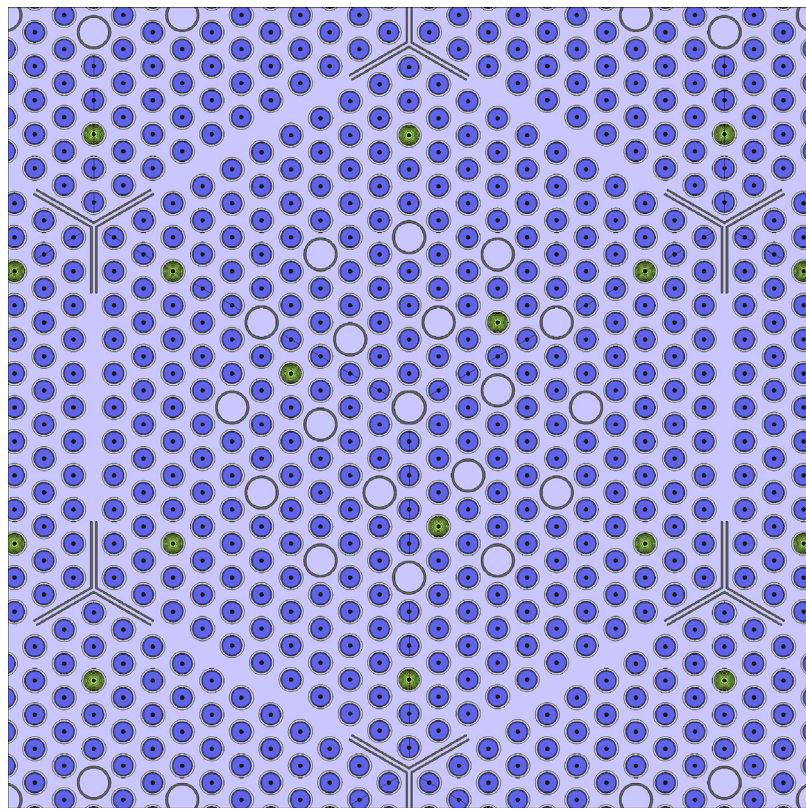


Fig. 3. Serpent geometry plot of assembly type 30AV5 in the infinite periodic lattice used for the homogenization of fuel assemblies.

Table 2

Burnup points (MWd/kgU) at which nominal group constants were evaluated. The burnup points used for off-nominal branch calculations are underlined.

0	0.1	0.3	0.6	1	1.5				
2	3	<u>4</u>	5	6	7	<u>8</u>	9	10	
11	<u>12</u>	13	14	15	<u>16</u>	17	18	19	<u>20</u>
24	27	<u>30</u>	33	36	<u>39</u>	42	<u>45</u>	48	51
								54	57
								59	<u>60</u>

Table 3

Group boundaries of the eight group structure.

20 MeV	821 keV	5.53 keV	4 eV	0.625 eV	0.28 eV	0.14 eV	58 meV	10 μ eV

The history calculations used the power density specified for the group constant generation part of the benchmark (42.5 W/gU) and applied the equilibrium xenon calculation option in Serpent. The branch calculations for hot full power (HFP) group constants used the xenon and samarium distributions from the history calculations whereas the branch calculations for hot zero power (HZP) group constants used zero xenon with samarium distribution from the history calculation.

Group constants were evaluated at the nominal branch conditions at 39 burnup points between 0 and 60 MWd/kgU, whereas the off-nominal branch calculations were only conducted at 11 burnups. This reduces the number of somewhat costly Monte Carlo transport solutions without a major penalty in accuracy assuming that the polynomial coefficients describing the dependence of the group constants on state parameters have a smooth dependence on burnup. The burnup points used in group constant generation are collected in [Table 2](#).

Serpent calculated the fuel assembly group constants into an intermediate 70 energy group structure, from which they were further condensed to the eight group structure shown in [Table 3](#) using the infinite flux spectrum. No critical spectrum correction was applied in these calculations based on the comparison conducted for the fresh core analyses ([Valtavirta et al., 2022a](#)).

The diffusion coefficients for the fuel assemblies were evaluated with the Cumulative Migration Method (CMM) ([Liu et al., 2018b](#)) using the direct group-wise approach described by [Liu et al. \(2018a\)](#).

Due to the periodic boundary conditions used in the hexagonal infinite lattice model, the assembly discontinuity factors (ADFs) could not be obtained directly from the Serpent simulation. The heterogeneous surface fluxes were instead tallied for the six sides of the assembly from the Serpent calculation along with current boundary conditions at the surfaces. The homogeneous surface fluxes were obtained from a single node Ants calculation based on the group constants and current boundary conditions tallied by Serpent.

4.2.4. Axial reflector homogenization

The axial reflector was homogenized using 4×10^9 active neutron histories with 500 inactive cycles over cylindrical regions ($R = 140$ cm) below and above of the active core in a 3D full core model. The uniform fission sites approach was used for variance reduction to move some of the source neutrons closer to the core axial boundaries.

4.2.5. Radial reflector homogenization

Radial reflectors were homogenized from a full core two-dimensional model using 4×10^9 active neutron histories with 500 inactive cycles. The uniform fission sites approach was used for variance reduction in the simulation to produce better statistics scores at the core periphery.

During the group constant post processing, the node and surface group constant data for the radial reflector positions was averaged between the different core symmetry sectors. Six symmetry sectors with periodic boundary conditions were used yielding eight unique radial reflector positions. The fuel side discontinuity factors for the reflector nodes were evaluated based on the surface flux data. The reflector discontinuity factors were corrected ([Smith, 2017](#)) with the ratio of the fuel side 2D infinite lattice ADF and the one calculated from the full core solution. The process has been described previously in detail ([Valtavirta et al., 2021, 2022b](#)).

4.2.6. Common options for group constant generation

The reflector group constants were evaluated without the fuel temperature branches at zero burnup.

The diffusion coefficient for radial and axial reflector nodes was the out-scatter diffusion coefficient, where transport correction (TRC) was applied for ^1H in H_2O .

All Serpent calculations used Doppler broadening rejection correction (DBRC) for ^{234}U , ^{235}U , ^{238}U , ^{239}Pu and ^{240}Pu between 0.1 eV and 1 keV. Probability table sampling for unresolved resonances was switched on. The nuclear data library used in the Serpent calculations was based on ENDF/B-VII.1.

The reflector homogenization calculations use a significantly higher number of active neutron histories compared to the fuel assembly homogenization due to the homogenized volumes (reflector regions) only constituting a part of the whole calculation geometry in the reflector homogenization meaning that only a small part of the modelled neutron interactions contribute to the group constants of any specific reflector region. The fact that the neutron flux distribution is focused on the active core instead of the reflector regions accentuates this problem.

4.3. Fuel cycle simulations

The time points (EFPD) for the fuel cycle simulation were taken from the tabulated cycle data in Lötsch et al. (2010) along with values for

- Reactor power.
- Feedwater flowrate.
- Feedwater inlet temperature.
- Position of control rod group 10.

This input data was used in the fuel cycle simulation assuming the data from time t_n to be held constant until the next tabulated time t_{n+1} . 3 % of coolant flow was directed to bypass, i.e. the flow rate through the active core was set to 97 % of the tabulated value.

The time integration in the burnup simulation used the predictor corrector method with constant extrapolation on the predictor and linear interpolation on the corrector step. The time integration on the corrector step was divided into ten substeps.

A 21 day decay time was modelled in between the fuel cycles to account for decay of the tracked nuclides during the fuel reloading. In addition to restarting the necessary nodal neutronics data based on the previous cycles, the fuel state for the SuperFINIX fuel behaviour solver was initialized based on restarts written at the end of the previous cycles.

5. Results

The predictions of Kraken for the fuel cycle simulations and start-up tests are presented in this section. Predicted values are compared to measured or reconstructed benchmark reference data as well as several computational predictions (bold text is used as headings in presented tables):

- **Benchmark** computational predictions that included results from five participating code systems (BIPR, DYN3D-Nessel, DYN3D-CASMO, DYN3D-Helios and TRAPEZ) as published by Lötsch et al. (2016).
- **SIMULATE5-HEX** as published by Bahadir (2018).
- **STREAM/RAST-V** as published by Jang et al. (2022).

In comparisons of single valued data such as single point critical boron, scram worth or isothermal temperature coefficient the difference between predicted and reference values (Delta) will be presented:

$$\text{Delta} = \text{Predicted} - \text{Reference}$$

Table 4

Differences between predicted and measured boron (g/kg) during the four cycles. SIMULATE5 results did not include low power points in the RMS.

	Ants		RAST-V	SIMULATE5	Benchmark
	Mean	RMS	RMS	RMS	RMS range
Cycle 1	-0.03	0.13	0.13	0.27	0.24 – 0.54
Cycle 2	-0.13	0.17	0.06	0.21	0.32 – 0.47
Cycle 3	-0.22	0.25	0.11	0.14	0.24 – 0.48
Cycle 4	-0.10	0.28	0.27	0.42	0.63 – 0.88
RMS of RMS		0.22	0.16	0.28	0.47 – 0.59

In comparisons extending over a large number of data points i , such as in boron letdown or power distribution comparisons, the root mean square (RMS) of the Delta is presented instead:

$$\text{RMS} = \sqrt{\frac{1}{N} \sum_{i=1}^N (\Delta_{i,i})^2}$$

For the computational predictions of the five benchmark code systems, the range of results is presented instead of the five results being presented separately.

The boron concentration in VVER reactors is commonly reported in grams of boric acid per a kilogramme of coolant (g/kg). This can be converted to the unit of weight ppm of boron in coolant commonly used in PWR context through (Bilodid et al., 2020):

$$C_B(\text{ppm}) = 174.88 \frac{\text{ppm}}{\text{g/kg}} \times C_B(\text{g/kg})$$

5.1. Boron letdown

The four fuel cycles were simulated with Kraken with the fuel shuffling modelled between the cycles. The predicted and measured boron letdown curves of the four fuel cycles are shown in Fig. 4. The agreement between Ants prediction and measured data largely stays in the ± 50 ppm range with cycles 3 and 4 showing the largest differences in visual inspection. Cycle 4 notably shows a large reactivity swing with an overprediction of critical boron of approximately 50 ppm in the beginning of the cycle and an underprediction of a similar magnitude in the end of the cycle. Similar reactivity swings can be observed in the cycle 4 boron letdown predictions of RAST-V and SIMULATE5. However, a similar behaviour is not seen in the results of the original benchmark participants in Fig. 15 of Lötsch et al. (2016).

Tabulated results of the differences between predicted and measured boron concentrations are collected in Table 4. The Ants results include the mean difference and the root mean square (RMS) of the difference for each four fuel cycles. RMS values of the differences of other code systems are included for comparison. RAST-V results are from Table 10 of Jang et al. (2022). SIMULATE5 results are from Table 1 of Bahadir (2018) and compared the hot full power predictions in only full power data points. Benchmark results are from Table 2 of Lötsch et al. (2016) and show the range of accuracy among the five participating codes.

The accuracy of the boron letdown prediction by Ants is comparable to that of the other nodal codes. The more recent solutions by Ants, RAST-V and SIMULATE5 generally perform better than the codes that participated in the original benchmark.

5.2. Power distributions during cycles

Subtask 2.2 of the benchmark involved evaluating the axially integrated fuel assembly power distribution in the core during each cycle at the beginning of cycle (BOC), middle of cycle (MOC) and end of cycle (EOC). Reconstructed power distributions based on self powered neutron detector (SPND) readings were provided for comparison in the benchmark. The reconstructed power distributions were normalized to a mean assembly power of 1.0 as was the assembly power distribution

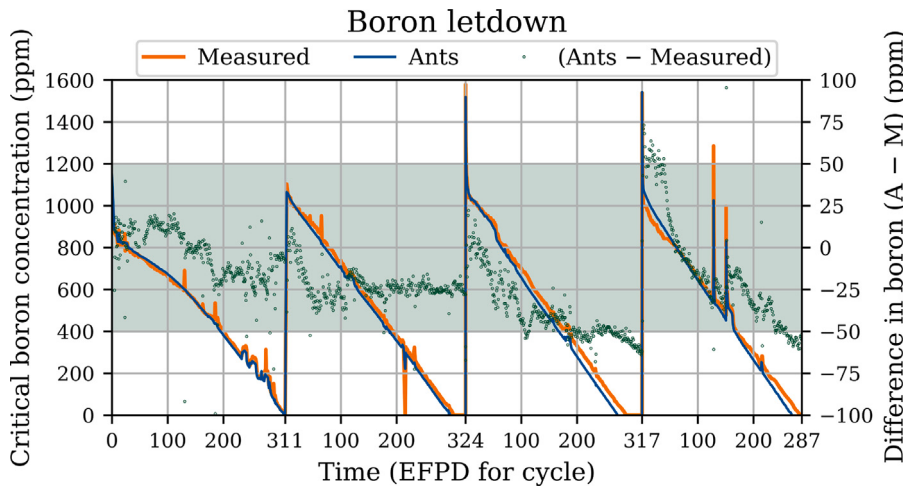


Fig. 4. Predicted and measured critical boron concentrations over the four fuel cycles and the absolute difference between the two. Shaded area indicates a ± 50 ppm range.

Table 5
Time points (effective full power days) for the comparisons of power distributions.

	BOC	MOC	EOC
Cycle 1	29.5	148.2	264.2
Cycle 2	29.0	105.8	218.5
Cycle 3	90.1	168.8	268.9
Cycle 4	3.1	134.8	216.9

predicted by Ants in these comparisons. The effective full power days at the different points of comparison are collected in Table 5.

The reconstructed assembly power distribution and Ants prediction are shown in Fig. 5 at the beginning of cycle 2. The accuracy of the Ants prediction at this time point was close to the average (RMS) accuracy of Ants in the twelve compared time points. The assemblies with self powered neutron detectors use bold font in these figures. It should be noted that the reconstructed data was only available up to two decimal points. The Ants results, available at higher precision are rounded to the precision of 0.01 for this figure.

The relative and absolute differences between the reconstructed and predicted normalized fuel assembly power distributions are shown in Fig. 6. In the evaluation of the differences, the reconstructed distribution serves as the reference with the differences evaluated using the full precision of the Ants results and the available precision of the reconstructed data (up to two decimal places). This means that the results of Fig. 6 cannot be directly calculated from the data presented in Fig. 5. The RMS of the relative difference in this point was 1.49% and the RMS of the absolute difference was 1.47 parts per one hundred.

The root mean square values of the relative differences in the normalized assembly power distribution are collected in Table 6. The RMS of the Ants results ranges from 0.92% to 2.15% with the RMS over all compared points being 1.36%. The benchmark results are based on Table 4 of Löttsch et al. (2016). On average (RMS of RMS), the Ants based calculation sequence of Kraken performs better than the benchmark participating codes, but Ants does not outperform all benchmark codes in all points of comparison.

The benchmark also included comparisons for the axial power distribution in specific fuel assemblies at BOC, MOC and EOC of the four fuel cycles. The reconstructed reference data is available for 10 equidistant axial layers in the core, which has been further linearly processed into 20 layers for the benchmark comparisons. As the axial nodalization in the Ants solution did not follow this equidistant nodalization a direct comparison between the Ants results and reconstructed data cannot be made.

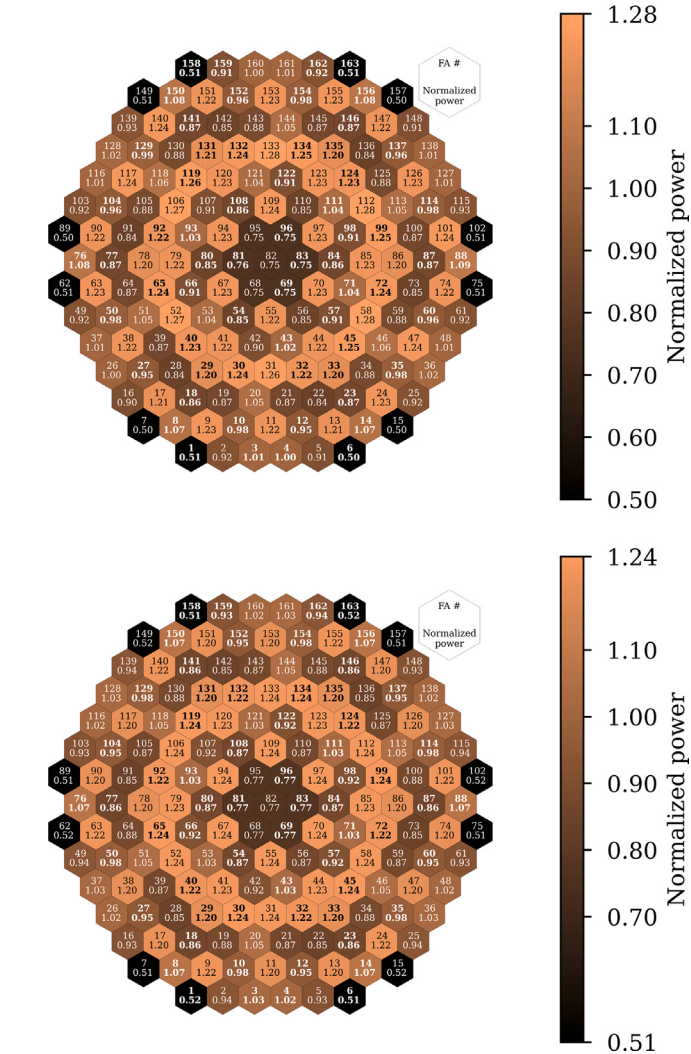


Fig. 5. Reconstructed (top) and Ants (bottom) normalized fuel assembly power distributions at BOC of cycle 2. Bold font indicates an assembly instrumented with self powered neutron detectors.

In order to illustrate the axial power distribution calculated by Ants and the reconstructed data, the distributions are shown in Fig. 7 for two

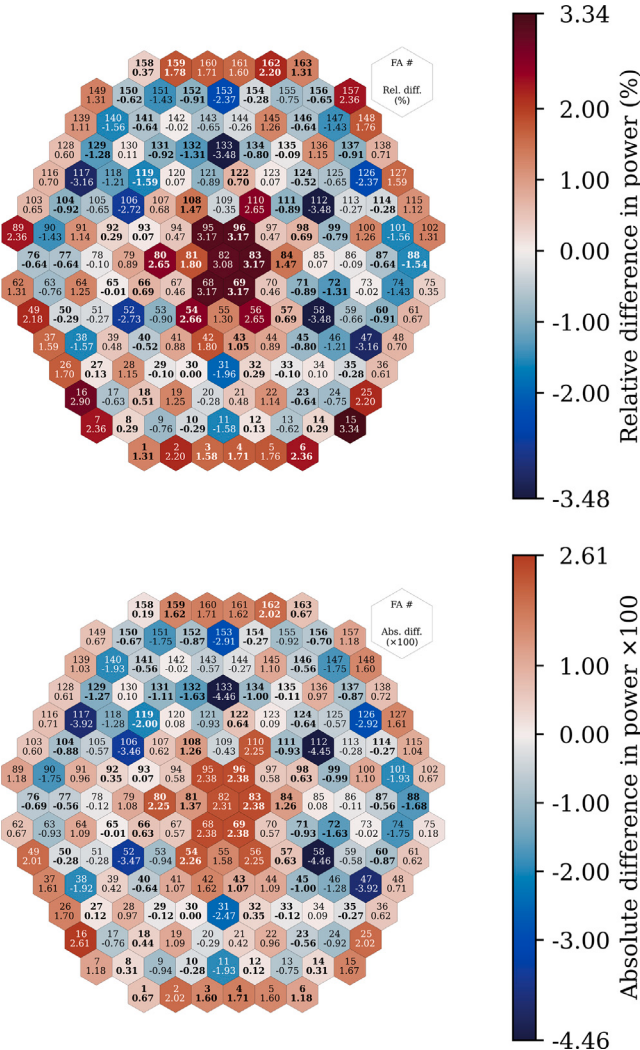


Fig. 6. Relative (top) and absolute (bottom) differences in normalized fuel assembly power distributions between Ants and reconstructed data at BOC of cycle 2. Bold font indicates an assembly instrumented with self powered neutron detectors.

Table 6
Root mean square of relative differences (percent) in fuel assembly power distributions between predicted and reconstructed.

	Ants RMS	Benchmark RMS range
BOC 1	1.49	1.34 – 2.83
MOC 1	0.92	1.00 – 1.38
EOC 1	1.00	0.68 – 1.16
BOC 2	1.49	1.30 – 2.23
MOC 2	1.13	1.24 – 1.67
EOC 2	0.95	0.82 – 1.12
BOC 3	2.15	2.96 – 3.66
MOC 3	1.23	1.64 – 2.22
EOC 3	1.28	0.93 – 1.24
BOC 4	1.05	1.88 – 3.04
MOC 4	1.23	1.32 – 1.85
EOC 4	1.83	1.20 – 1.76
RMS of RMS	1.36	1.72 – 1.96

fuel assemblies at the same BOC of cycle 2 as the fuel assembly powers that were shown in Figs. 5 and 6. Fuel assembly #82 is the central fuel assembly in the core, whereas fuel assembly #102 is situated at the core periphery. The reconstructed data is plotted at the midpoints of the 10

axial layers. Ants axial power densities have been plotted separately simply as normalized to an average full core power density of unity (Ants) and scaled with the relative difference of the local assembly power (Ants, scaled). Based on visual inspection, Ants reproduces the axial power shapes well.

5.3. Start-up tests

The start-up tests conducted at the beginning of each fuel cycle were modelled with the Ants based calculation sequence of Kraken starting from either the fresh core for fuel cycle 1 or the shuffled and reloaded core for cycles 2–4. The tests were modelled using the benchmark specifications of the thermal hydraulic states.

5.3.1. Critical boron at hot zero power

The critical boron comparisons for Ants are made against the critical states defined in the benchmark specifications. Cycle 1 critical state is taken from the revised specifications (Bilodid et al., 2020), whereas critical states for cycles 2–4 are taken from earlier specifications (Lötsch et al., 2016). The results are presented in Table 7. The differences between measured and predicted values for SIMULATE5 are taken from Table 2 of Bahadir (2018), whereas the calculated benchmark results provide the range of the differences from Table 7 of Lötsch et al. (2016). It should be noted that the measured values reported with the SIMULATE5 results do not exactly agree with the ones in this table and are likely from a different revision of the specifications. This is likely the case also with the calculated benchmark results. RMS of Delta for benchmark codes (last row of last column) show the minimum and maximum of the RMS differences among the benchmark codes.

Based on this comparison, the Ants based calculation sequence predicts the initial core hot zero power critical boron very well. The accuracy (RMS of Delta) of Ants, SIMULATE5 and the most accurate of the benchmark participating codes was close to 0.10 g/kg corresponding to a smaller than 20 ppm difference between predicted and measured boron concentration.

It is interesting to note that the accuracy of Ants is generally better for the start-up hot zero power boron concentrations than for the boron letdown during the operating cycles. While the group constant model only explicitly models the decay of a small number of short lived nuclides during the modelled 21 day outage period, the critical boron after the decay is predicted well.

5.3.2. Partial and full scram worth

The partial and full scram worths of the control rods were measured at the start of each cycle. Partial scram worth measurement excluded the highest worth control rod assembly. The measured data and Ants predictions are collected in Table 8 along with the differences for predicted and measured scram worths from other codes. The RAST-V results are from Table 14 of Jang et al. (2022). Table 9 and 10 of Lötsch et al. (2016) show the relative differences between predicted and measured net (partial) and gross (full) scram worths of the participating codes. The absolute pcm differences for the benchmark codes have been calculated for this table by multiplying the relative difference with the measured reactivity worth.

All nodal codes clearly overpredict the reactivity worths compared to the measured data. This is a known challenge in VVER-1000 reactivity measurements even when calculated with Monte Carlo codes (Bilodid et al., 2020). The approach of estimating the reactivity based on inverse point-kinetic fitting to time-dependent detector signals from outside the reactor pressure vessel has its limitations and introduces some systematic errors in the measured values as described by Afanasiev and Pinegin (2014). Ants predictions are in line with those of the other nodal codes.

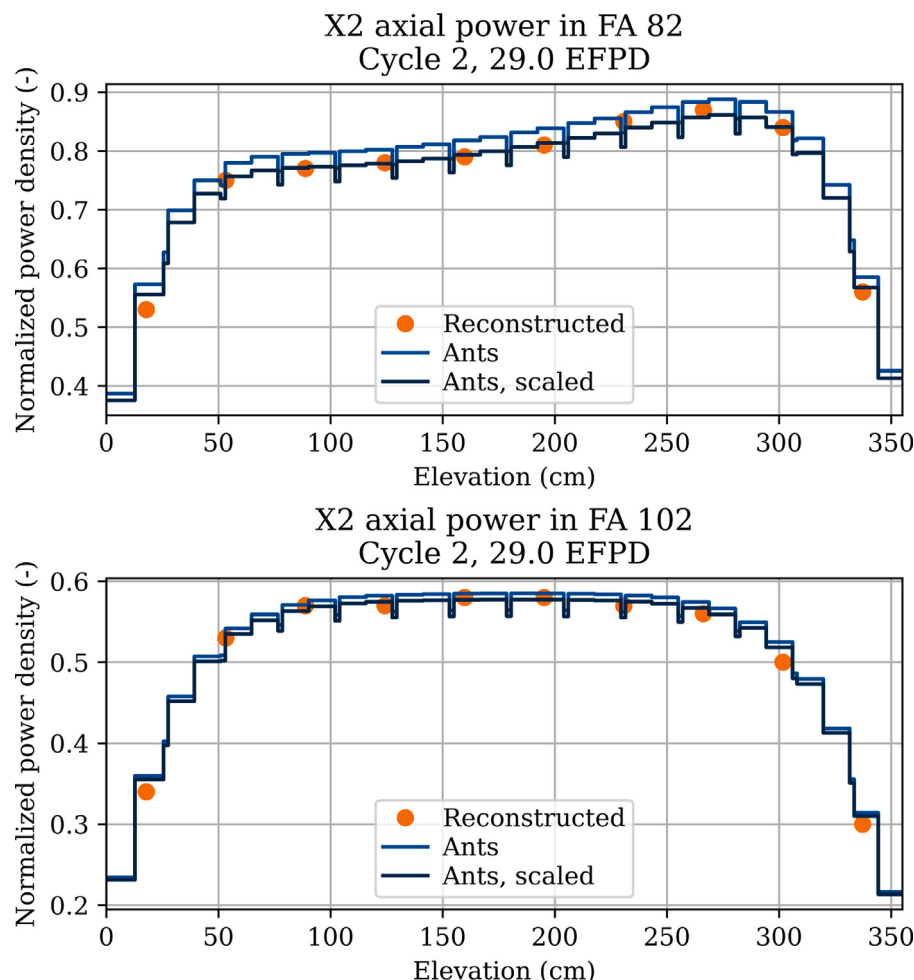


Fig. 7. Ants normalized nodal power density and reconstructed axial power distribution for fuel assemblies #82 and #102 at BOC of cycle 2.

Table 7
Predicted and measured critical boron (g/kg) for the hot zero power state at the beginning of each cycle. Initial state of the first isothermal temperature reactivity coefficient test.

	Measured	Ants	Ants Delta	SIMULATE5	Benchmark
				Delta	Delta range
Cycle 1	6.90	6.93	+ 0.03	+ 0.05	-0.23 – + 0.08
Cycle 2	8.81	8.77	-0.04	-0.09	-0.37 – + 0.10
Cycle 3	8.96	8.81	-0.14	-0.03	-0.39 – + 0.33
Cycle 4	8.96	9.06	+ 0.10	+ 0.18	-0.63 – -0.13
RMS of Delta			0.09	0.10	0.11 – 0.41

Table 8
Predicted and measured scram worth (pcm) at the start of each cycle. C1, full measured worth is taken from 2022 fresh core specifications update. Value in earlier benchmark specifications was 6960 pcm.

	Measured	Ants	Ants Delta	RAST-V	Benchmark
				Delta	Delta range
C1, partial	5230	5745	+ 515	+ 573	+ 380 – + 860
C1, full	7000	7616	+ 656	+ 596	+ 272 – + 1308
C2, partial	5590	6412	+ 822		+ 420 – + 990
C2, full	6760	7826	+ 1066		+ 525 – + 1190
C3, partial	5680	6813	+ 1133		+ 917 – + 1500
C3, full	7320	8589	+ 1269		+ 979 – + 1690
C4, partial	4840	5499	+ 659		+ 710 – + 1160
C4, full	6260	7342	+ 1082		+ 926 – + 1550
RMS of Delta			936		720 – 1306

Table 9

Predicted and measured isothermal temperature reactivity coefficient (pcm/K) at the start of each cycle. The measured values for C1T1 and C1T2 are taken from the cooling part of the test.

	Measured	Ants	Ants Delta	RAST-V	SIMULATE5	Benchmark
				Delta	Delta	Delta range
C1T1	-6.7	-6.0	+ 0.7	+ 0.1	+ 0.2	-0.5 – + 3.6
C1T2	-18.6	-14.0	+ 4.6	+ 4.7	+ 2.9	-2.9 – + 0.2
C2T1	-10.5	-9.1	+ 1.4	+ 4.5	+ 2.4	-1.1 – + 3.6
C2T2	-4.3	-6.1	-1.8	+ 1.5	+ 0.1	+ 1.4 – + 6.4
C3T1	-11.6	-12.6	-1.0	+ 2.4	+ 0.7	-0.4 – + 4.6
C3T2	-9.3	-9.8	-0.5	+ 2.9	+ 1.6	-0.1 – + 4.1
C4T1	-15.4	-15.2	+ 0.2	+ 2.9	+ 1.5	-2.0 – + 3.4
C4T2	-12.0	-12.4	-0.4	+ 2.4	+ 1.4	-0.9 – + 3.8
RMS of Delta			1.9	3.0	1.6	1.2 – 3.9

5.3.3. Isothermal temperature reactivity coefficient

The isothermal reactivity coefficient for the core was measured in two different control rod configurations at the start of each cycle. The measurements consisted of perturbing the core temperature from an initial state, followed by a return to the initial state. For cycle 1 the tests at both control rod configurations reported two distinct values, one from cooling the core and one from returning the core to the original state. While these perturbations are equivalent in the simulations, the measured values differed. The values included in Table 9 as a reference (measured) are based on the downward (cooling) part of the perturbation. RAST-V results are from Table 15 of Jang et al. (2022) and the Delta values have been rounded to one decimal from the reported two decimal values. SIMULATE5 results are from Table 3 of Bahadir (2018). Calculated benchmark results provide the range of the differences from Table 8 of Lötsch et al. (2016).

5.3.4. Reactivity worth curve for the working control rod group

The last measurement of the physics tests investigated here is the integral and differential worth measurement of the working control rod group (#10). Groups 1 – 9 were withdrawn in the measurements with group 10 starting from a fully or partially inserted position. The group was extracted by steps with the inserted reactivity being measured and the boron concentration being increased during the process. The measured data is available for the first cycle as integral and differential worths at specific extraction points between 0 % and 72 % withdrawn. For cycles 2–4 the reactivity changes associated with a specific control rod movement, for example from 21 % to 25 % withdrawn, are given instead. Moreover, for cycles 2–4 group 10 does not start the experiment fully inserted.

Ants was used to evaluate integral and differential control rod worths at the start of each cycle. The solution was first converged to obtain the critical boron at the starting conditions, followed by multiple steps of extraction of group 10. The boron concentration was not recalculated during the control rod extraction process with Ants, which is not expected to have a noticeable effect on the results.

The measured and predicted integral worth curves are compared in Fig. 8 whereas the differential worth curves are shown in Fig. 9. To investigate potential cusping effects in the reactivity worth evaluation, the calculation was conducted once using the control rod movements reported in the measured data and a second time using control rod movements coinciding with Ants axial node boundaries. Based on visual inspection, the accuracy of the Ants predictions is similar to that of the nodal codes participating in the X2 benchmark presented in Figures 16–19 of Lötsch et al. (2016). Cusping effects can be seen in the differential worth curves, especially for cycles 2 and 3 as a sawtooth behaviour around 75 % extraction. Such effects are not reflected to the integral worth curves. The measured data for the differential worths shows some uneven behaviour, which may indicate the level of experimental uncertainty.

Root mean square values calculated for the relative reactivity differences between predicted and measured data for each cycle are shown in Table 10. The predicted data includes the possible control rod cusping

Table 10

RMS relative differences between predicted and measured (Ants) or predicted and mean (Benchmark) worth of CR10 at the start of each cycle.

	Integral worth		Differential worth	
	Ants	Benchmark	Ants	Benchmark
	RMS	RMS range	RMS	RMS range
Cycle 1	15.5	8.3 – 23.7	17.3	9.1 – 30.5
Cycle 2	7.6	5.2 – 18.7	16.6	6.0 – 28.4
Cycle 3	11.2	12.3 – 22.7	9.2	3.6 – 33.8
Cycle 4	3.4	11.7 – 18.5	9.5	4.8 – 40.0
RMS of RMS	10.4	11.3 – 19.2	13.7	12.6 – 30.2

errors. As opposed to the Ants results, which are compared against the experimental measurements, the benchmark results are compared against the mean value of the calculated results and are taken from Tables 11 and 12 of Lötsch et al. (2016). The differences between Ants and measured values are of similar magnitude than the differences between the benchmark participants and the mean value of benchmark participants. The spread in the computational benchmark results is rather large. The introduction of an axial homogenization methodology in Ants is likely to change these results in the future.

5.4. Group constant modelling effects

The results presented in the previous section were obtained with eight energy groups and no leakage correction applied in the generation of fuel assembly group constants. Based on results obtained for the hot zero power states of the X2 fresh core (Valtavirta et al., 2022a) this was expected to yield the best accuracy. In order to test this hypothesis, two group constants were condensed from this work's eight group constants and the analyses were repeated with data. The effect of using the Fundamental Mode based leakage correction for fuel assembly data was also studied. All in all, this led to the comparison between four sets of results:

1. **Ref.:** The reference results, presented in Section 5. Eight energy groups, no leakage correction (infinite spectrum data for fuel assemblies).
2. **V1:** Eight energy groups, leakage correction used for fuel assembly data.
3. **V2:** Two energy groups, leakage correction used for fuel assembly data.
4. **V3:** Two energy groups, no leakage correction (infinite spectrum data for fuel assemblies).

The results are compared in a condensed form, including all of the results presented in the previous section except the SCRAM worths due to the known biases in their measurements and the differential control rod worths due to the cusping effects in the calculated values.

- **Boron:** Critical boron letdown curves, RMS of absolute differences (g/kg) over all points over all cycles.

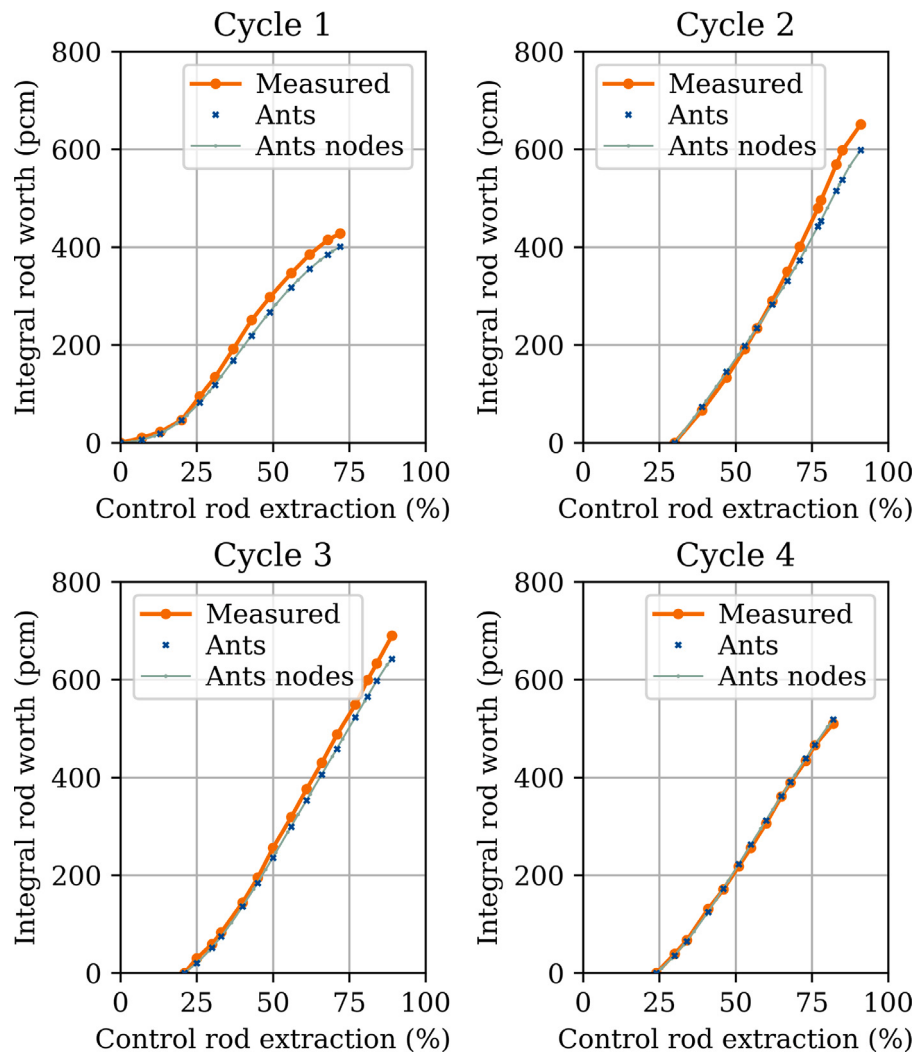


Fig. 8. Measured and predicted integral worths for control rod group 10 at the start of each cycle. Predictions either based on actual reported control rod movements (Ants) or on control rod movements coinciding with Ants axial node boundaries (Ants nodes).

Table 11
Effect of variations on errors between predicted and measured data. LC and ∞ refer to using leakage corrected or infinite spectrum data for fuel assembly group constants.

	Error				Error relative to Ref.		
	Ref.	V1	V2	V3	V1	V2	V3
	8 g ∞	8 g LC	2 g LC	2 g ∞	8 g LC	2 g LC	2 g ∞
Boron	0.22	0.22	0.21	0.19	1.00	0.95	0.86
FA powers	1.36	1.44	1.65	1.77	1.06	1.21	1.30
HZP boron	0.09	0.09	0.09	0.10	1.00	1.00	1.11
ITC	1.87	1.89	1.96	1.83	1.01	1.05	0.98
ICRW	10.4	9.3	9.3	13.3	0.89	0.89	1.28

- FA powers:** Axially integrated fuel assembly power distributions, RMS of relative differences (%) over all 12 time points and all 163 fuel assemblies.
- HZP boron:** Critical boron at the hot zero power tests, RMS of absolute differences (g/kg) over all four tests (one test per cycle).
- ITC:** Isothermal reactivity coefficients, RMS of absolute differences (pcm/K) including two tests at the start of each four cycles.
- ICRW:** Integral control rod worths, RMS of relative differences (%) including all measurements for all cycles.

The errors for each group constant set are presented in Table 11. The left side of the table presents the errors whereas the right side presents the relative magnitude of each error compared to that obtained with the reference group constants. The number of energy groups and the use

of leakage correction does have an effect on the results: In variation V1, the use of leakage correction with eight energy groups does not have a large effect on the evaluation of the reactor reactivity (Boron, HZP boron or ITC), but is slightly detrimental to the evaluation of the fuel assembly power distribution. The errors in the integral control rod worth evaluation are reduced by approximately 10 %. Variation V2, the use of leakage corrected two group data improves the errors on the boron letdown curves by 5 % with a clear degradation of the FA power distribution. The hot zero power borons are unaffected. Variation V3, the two group data in infinite spectrum yields further improvements to the boron letdown curve, even worse results for the fuel assembly power distribution and perhaps counterintuitively a degradation for the hot zero power boron concentrations.

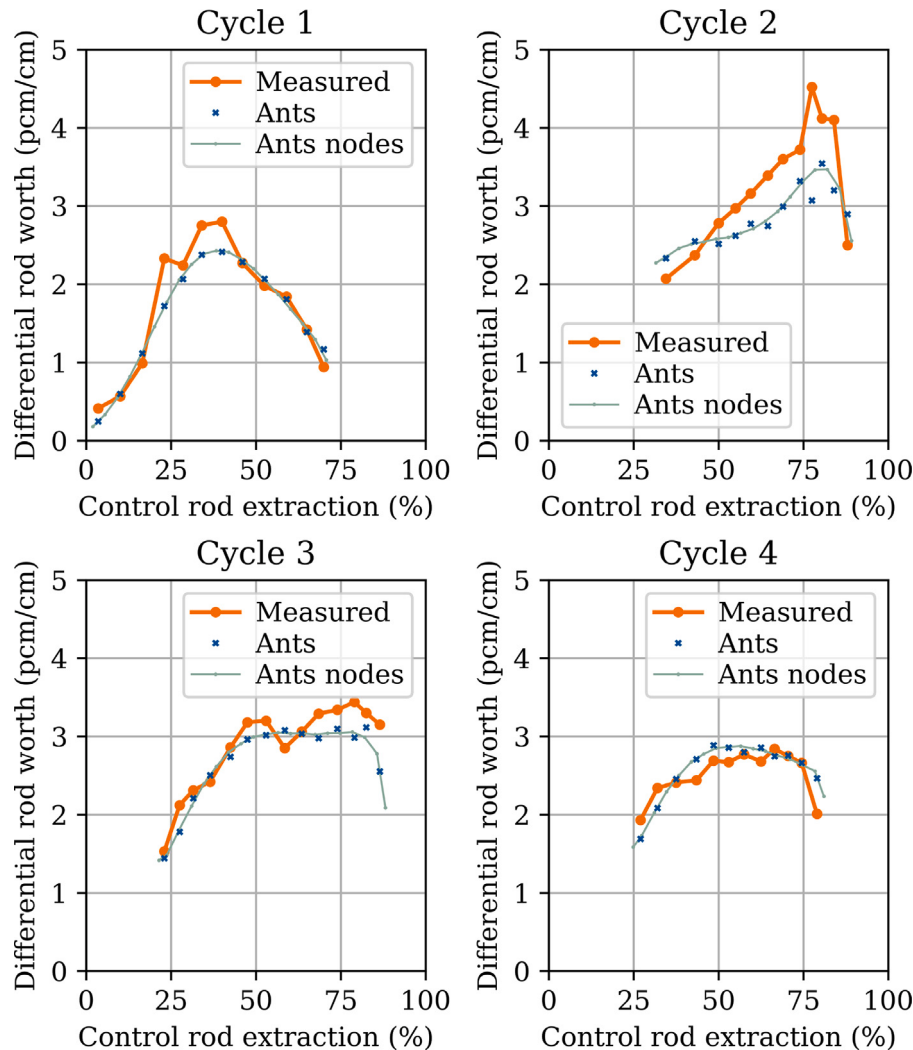


Fig. 9. Measured and predicted differential worths for control rod group 10 at the start of each cycle. Predictions either based on actual reported control rod movements (Ants) or on control rod movements coinciding with Ants axial node boundaries (Ants nodes).

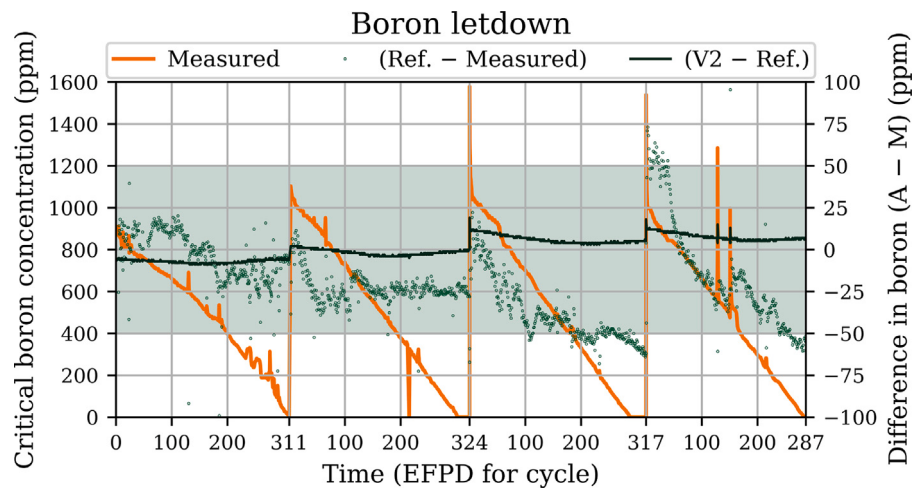


Fig. 10. Measured critical boron concentrations over four cycles, the predictive error of the reference group constant set (Ref.) and the effect of switching from Ref. to V2 group constants (V2 - Ref.).

A more detailed investigation for the effects of the two group data on boron letdown curves is presented in Fig. 10. The Figure

shows the effect on the predicted critical boron concentrations when changing from the Ref. group constant set to the two-group leakage

corrected data (V2). The reference data underpredicts the critical boron concentration on average. The V2 data set decreases accuracy for cycle 1, does not affect it for cycle 2 and somewhat improves it for cycles 3 and 4. The improvements seen for the V3 data set were found to be largely the result a rather constant increase in core reactivity. The swings in the predictive accuracy observed during the operating cycles were not reduced by the two-group data.

No set of group constants produces the lowest errors for all investigated output quantities. The reference group constants are the most accurate for predicting the assembly power distribution, whereas two group constants provide a better match for the boron letdown with a significant degradation in the assembly power distribution. The results are in line with the previous analyses for the X2 hot zero power state, but the good performance of the two group data regarding the boron concentrations during operation could not be predicted based on the fresh core comparison.

6. Discussion and future work

This work evaluated the capability of Kraken to model VVER-1000 fuel cycles, including operation at reduced power levels and fuel shuffling and reloading between the fuel cycles. The Ants based calculation sequence performed well in modelling the fuel cycles and start-up tests in the X2 benchmark. Comparisons of various quantities predicted by Kraken with measured and reconstructed data showed differences well in line with other nodal diffusion based codes. The comparisons against reference data provides quantitative estimates of the accuracy of the calculation sequence in such analyses. Anticipated operational occurrences or transient scenarios were not covered in this work and the applicability of Kraken for such analyses needs to be established separately.

Future analyses may focus on the transient scenarios included in the X2 benchmark, namely reactor scram, xenon oscillations and the switching off of one of the main circulation pumps. The modelling of system scale transient scenarios for VVER-1000 reactors is also ongoing using the coupling between Ants and the system code TRACE within the Kraken framework (Lauranto et al., 2023).

In addition to the hexagonal nodal model, Ants supports a triangular nodalization of the hexagons, which would allow tracking nodal data such as burnups and nuclide concentrations at a higher spatial resolution than was achieved with the hexagonal nodes. The generation of proper group constants for the triangular nodal model, including discontinuity factors as well as the extension of the fuel cycle simulation sequence to include the triangular nodal model would allow the validation of the triangular nodal model in a similar manner in the future.

The accuracy of Ants pin power predictions in hexagonal lattice calculations has been evaluated against Serpent reference solutions in fresh core zero power conditions (Valtavirta et al., 2022b), but the analyses have not yet been extended to depleted systems or full power operation. Subtask 3.2 of the X2 benchmark focuses on the prediction of the pin power distributions of selected assemblies at different points during the four fuel cycles with computational reference results provided.

The start-up tests were modelled with a separate set of group constants generated around the hot zero power state. Extending the group constant generation set up to produce a single wide range group constant library that can be applied for both normal operation and shutdown analyses is a further future development goal.

CRediT authorship contribution statement

Ville Valtavirta: Software, Methodology, Investigation, Conceptualization, Formal analysis, Visualization, Writing – original draft, Writing – review & editing. **Antti Rintala:** Software, Methodology, Conceptualization, Writing – original draft, Writing – review & editing.

Declaration of competing interest

The authors declare that they have no known competing financial interests or personal relationships that could have appeared to influence the work reported in this paper.

Data availability

Data will be made available on request.

Acknowledgements

The authors thank Thomas Lötsch for providing the reference data and specifications for the X2 benchmark.

This work has received funding from the LONKERO project under the Finnish National Research Programme on Nuclear Power Plant Safety, SAFIR2022.

This work has received funding from the DECAPOD project under the Finnish National Nuclear Safety and Waste Management Research Programme 2023–2028, SAFER2028.

References

- Afanasiev, D., Pinegin, A., 2014. Comparison of the accuracy of different methods of measuring the effectiveness of emergency protection system in VVER-1000. In: Proceedings of 24th Symposium of AER on VVER Reactor Physics and Reactor Safety. Sochi, Russia.
- Bahadir, T., 2018. SIMULATE5-HEX extension for VVER analyses. Kerntechnik 83, 268–274. <http://dx.doi.org/10.3139/124.110908>.
- Bilodid, Y., Fridman, E., Lötsch, T., 2020. X2 VVER-1000 benchmark revision: Fresh HZP core state and the reference Monte Carlo solution. Ann. Nucl. Energy 144, 107558. <http://dx.doi.org/10.1016/j.anucene.2020.107558>, URL: <https://www.sciencedirect.com/science/article/pii/S0306454920302565>.
- Bilodid, Y., Kotlyar, D., Margulis, M., Fridman, E., Shwageraus, E., 2015. Spectral history model in DYN3D: Verification against coupled Monte-Carlo thermal-hydraulic code BGCore. Ann. Nucl. Energy 81, 34–40. <http://dx.doi.org/10.1016/j.anucene.2015.03.030>, URL: <https://www.sciencedirect.com/science/article/pii/S0306454915001644>.
- Hirvensalo, M., Rintala, A., Sahlberg, V., 2021. Triangular geometry model for Ants nodal neutronics solver. In: Proceedings of the International Conference on Mathematics and Computational Methods Applied To Nuclear Science and Engineering. M&C 2021, Raleigh, North Carolina, USA.
- Ikonen, T., Loukusa, H., Syrjälähti, E., Valtavirta, V., Leppänen, J., Tulkki, V., 2015. Module for thermomechanical modeling of LWR fuel in multiphysics simulations. Ann. Nucl. Energy 84, 111–121. <http://dx.doi.org/10.1016/j.anucene.2014.11.004>, URL: <http://www.sciencedirect.com/science/article/pii/S0306454914005842>.
- Ingremea, J.-J., Taforeau, J., Tixier, G., Hébert, A., 2018. Impact of the samarium depletion chain modeling in a PWR equilibrium cycle using DRAGON and DONJON. In: PHYTRA4. Marrakech, Morocco.
- Jang, J., Dzianisau, S., Lee, D., 2022. Development of nodal diffusion code RAST-V for Vodo-Vodyanoi Energetichesky reactor analysis. Nucl. Eng. Technol. 54 (9), 3494–3515. <http://dx.doi.org/10.1016/j.net.2022.04.007>, URL: <https://www.sciencedirect.com/science/article/pii/S1738573322001929>.
- Kozlowski, T., Downar, T.J., 2006. The PWR Core Transient Benchmark, Final Report, NEA/NSC/DOC(2006)20. Technical Report NEA/NSC/DOC(2006)20, OECD/NEA.
- Lauranto, U., Komu, R., Rintala, A., Valtavirta, V., 2023. Validation of the Ants-TRACE code system with VVER-1000 coolant transient benchmarks. Ann. Nucl. Energy (accepted for publication).
- Leppänen, J., Mattila, R., 2015. Study on computational performance in generation of cross sections for nodal simulators using continuous-energy Monte Carlo calculations. J. Nucl. Sci. Technol. 52 (7–8), 945–952. <http://dx.doi.org/10.1080/00223131.2015.1027516>.
- Leppänen, J., Pusa, M., Viitanen, T., Valtavirta, V., Kaltainenaho, T., 2015. The Serpent Monte Carlo code: Status, development and applications in 2013. Ann. Nucl. Energy 82, 142–150. <http://dx.doi.org/10.1016/j.anucene.2014.08.024>, URL: <http://www.sciencedirect.com/science/article/pii/S0306454914004095>.
- Leppänen, J., Valtavirta, V., Rintala, A., Hovi, V., Tuominen, R., Peltonen, J., Hirvensalo, M., Dorval, E., Lauranto, U., Komu, R., 2022. Current status and on-going development of VTT's Kraken core physics computational framework. Energies 15 (3), <http://dx.doi.org/10.3390/en15030876>, URL: <https://www.mdpi.com/1996-1073/15/3/876>.
- Leppänen, J., Valtavirta, V., Tuominen, R., Rintala, A., Lauranto, U., 2021. A Finnish district heating reactor: Neutronics design and fuel cycle simulations. In: Proceedings of 2021 28th International Conference on Nuclear Engineering. ICONE28, Virtual, Online, URL: <https://asmadigitalcollection.asme.org/ICONE/proceedings/ICONE28/85246/V001T00A001/1122301>.

- Liu, Z., Chen, J., Li, S., Wu, H., Cao, L., 2022. Development and verification of the hexagonal core simulation capability of the NECP-X code. *Ann. Nucl. Energy* 179, 109388. <http://dx.doi.org/10.1016/j.anucene.2022.109388>, URL: <https://www.sciencedirect.com/science/article/pii/S0306454922004200>.
- Liu, Z., Smith, K., Forget, B., 2018a. Group-wise tally scheme of incremental migration area for cumulative migration method. In: Proceedings of PHYSOR 2018. Cancún, México.
- Liu, Z., Smith, K., Forget, B., Ortensi, J., 2018b. Cumulative migration method for computing rigorous diffusion coefficients and transport cross sections from Monte Carlo. *Ann. Nucl. Energy* 112, 507–516. <http://dx.doi.org/10.1016/j.anucene.2017.10.039>, URL: <https://www.sciencedirect.com/science/article/pii/S0306454917303778>.
- Lötsch, T., Khalimonchuk, V., Kuchin, A., 2009. Proposal of a benchmark for core burnup calculations for a VVER-1000 reactor core. In: Proceedings of the 19th AER Symposium on VVER Reactor Physics and Reactor Safety. Varna, Bulgaria.
- Lötsch, T., Khalimonchuk, V., Kuchin, A., 2010. Corrections and additions to the proposal of a benchmark for core burnup calculations for a VVER-1000 reactor. In: Proceedings of the 20th AER Symposium on VVER Reactor Physics and Reactor Safety. Helsinki, Finland.
- Lötsch, T., Kliem, S., Bilodid, E., Khalimonchuk, V., Kuchin, A., Ovdienko, Y., Ieremenko, M., Blank, R., Schultz, G., 2016. The X2 benchmark for VVER-1000 reactor calculations overview and current status. In: Proceedings of the 26th AER Symposium on VVER Reactor Physics and Reactor Safety. Helsinki, Finland.
- Papadionysiou, M., Kim, S., Hursin, M., Vasilev, A., Ferroukhi, H., Pautz, A., Joo, H.G., 2022. Verification and validation of the high-resolution code nTF with VVER-1000 hot zero power monte carlo calculations and experimental data. *Ann. Nucl. Energy* 178, 109385. <http://dx.doi.org/10.1016/j.anucene.2022.109385>, URL: <https://www.sciencedirect.com/science/article/pii/S0306454922004170>.
- Rintala, A., Lauranto, U., 2023. Time-dependent neutronics model of nodal neutronics program Ants. *Ann. Nucl. Energy* (accepted for publication).
- Rintala, A., Sahlberg, V., 2019. Extension of nodal diffusion solver of Ants to hexagonal geometry. *Kerntechnik* 84 (4), 252–261. <http://dx.doi.org/10.3139/124.190013>.
- Sahlberg, V., Rintala, A., 2018. Development and first results of a new rectangular nodal diffusion solver of Ants. In: Proceedings of PHYSOR 2018. Cancun, Mexico.
- Smith, K., 2017. Nodal diffusion methods and lattice physics data in LWR analyses: Understanding numerous subtle details. *Prog. Nucl. Energy* 101, 360–369. <http://dx.doi.org/10.1016/j.pnucene.2017.06.013>, URL: <https://www.sciencedirect.com/science/article/pii/S0149197017301609>.
- Tuominen, R., Valtavirta, V., 2023. BEAVRS pin-by-pin calculations with Ants-SUBCHANFLOW-SuperFINIX code system. *Ann. Nucl. Energy* 180, 109447. <http://dx.doi.org/10.1016/j.anucene.2022.109447>, URL: <https://www.sciencedirect.com/science/article/pii/S0306454922004777>.
- Valtavirta, V., Hovi, V., Loukusa, H., Rintala, A., Sahlberg, V., Tuominen, R., Leppänen, J., 2019a. Kraken – an upcoming Finnish reactor analysis framework. In: Proceedings of ANS M&C 2019. Portland, OR, USA.
- Valtavirta, V., Lauranto, U., Hovi, V., Peltonen, J., Rintala, A., Tuominen, R., Leppänen, J., 2020. High fidelity and reduced order solutions to an SMR-level progression problem with the Kraken computational framework. In: Proceedings of PHYSOR 2020. Cambridge, UK.
- Valtavirta, V., Lauranto, U., Rintala, A., 2022a. Evaluating the X2 initial core zero power physics tests with Serpent-Ants. In: Proceedings of PHYSOR 2022. Pittsburgh, PA.
- Valtavirta, V., Peltonen, J., Lauranto, U., Leppänen, J., 2019b. SuperFINIX – A flexible-fidelity core level fuel behavior solver for multi-physics applications. In: NENE 2019. Portorož, Slovenia.
- Valtavirta, V., Rintala, A., 2021. Specifications for the Generic Polynomial Group Constant Model of Ants. Technical Report VTT-R-00154-21, VTT Technical Research Centre of Finland Ltd.
- Valtavirta, V., Rintala, A., Lauranto, U., 2021. Validating the Serpent-Ants calculation chain using BEAVRS fresh core hot zero power data. *J. Nucl. Eng. Radiat. Sci.* <http://dx.doi.org/10.1115/1.4052731>.
- Valtavirta, V., Rintala, A., Lauranto, U., 2022b. Pin power reconstruction for hexagonal geometry in nodal neutronics program Ants. *Ann. Nucl. Energy* 179, 109384. <http://dx.doi.org/10.1016/j.anucene.2022.109384>, URL: <https://www.sciencedirect.com/science/article/pii/S0306454922004169>.
- Valtavirta, V., Tuominen, R., 2021. A simple reactor core simulator based on VTT's Kraken computational framework. In: Proceedings of ANS M&C 2021. Raleigh, North Carolina, USA.